Supporting Information

Vaithiyalingam et al. 10.1073/pnas.1002009107

SI Text

SI Methods. ***Proteins expression and production.*** Recombinant human primase heterodimer expression and purification was described previously (1). The p58C (residues 272–464) construct was subcloned into an in-house pBG100 vector (Dr. L. Mizoue, Center for Structural Biology) containing an N-terminal hexahistidine tag and H3C protease cleavage site. Protein was expressed in *Escherichia coli* BL21 (DE3) cells (Novagen) cultured at 37 °C to an OD_{600} of 0.6–0.7. Then 0.1 mg/mL of ferric citrate and 0.5 M of isopropyl 1-thio-β-D-galactopyranoside were added, and the cells were grown further at 18 °C overnight. Cells were resuspended in buffer containing 20 mM Tris (pH 8.0), 300 mM NaCl, 20 mM imidazole, and 0.1% NP40, and lysed using an Avestin EmulsiFlex C3 homogenizer. Protein was purified by nickel affinity chromatography (Amersham Biosciences), and after cleavage of the six histidine tag by H3C protease, by S75 and/or S200 gel filtration column (Amersham Biosciences). Mutants of p58C were generated using a Quick-Change Kit (Stratagene) and purified using a protocol similar to the wild-type protein. RPA32C was produced by the published procedure (2). To obtain ^{15}N-enriched NMR samples of p58C or RPA32C, the proteins were grown in a minimal medium supplemented with $^{15}NH_4Cl$ as the sole nitrogen source.

Crystallization and structure determination. Crystals were grown by sitting drop vapor diffusion at 21 °C from a drop composed of equal volumes of protein and reservoir solution containing 100 mM Tris (pH 8.5), 200 mM LiSO4, and 20% PEG 3350. Prior to data collection, crystals were soaked in mother liquor containing 20% glycerol and flash frozen in liquid nitrogen. X-ray data were collected on a laboratory rotating anode source and at sector 21 (Life Sciences Collaborative Access Team) at the Advanced Photon Source. All data were processed by HKL2000 (3). The crystals belong to space group C2 and contained two molecules in the asymmetric unit. The structure was determined using single-wavelength anomalous dispersion (SAD) phase information derived from in-house diffraction data collected at the Cu Kα-edge. The centroid position of the 4Fe-4S cluster was calculated from visual inspection of the Harker sections of the anomalous Patterson map. The program SHARP was used to refine the orientation of the cluster, calculate phases, and perform density modification (4). The atomic model was built into the experimentally phased 2.2 Å electron density map using the program Coot (5) and refined against 1.7-Å synchrotron diffraction data using Phenix (6). Electrostatic field potentials were calculated using Delphi (7). The structure has been deposited in the Protein Data Bank under accession code 3L9Q.

Fluorescence spectroscopy. The binding of DNA to wild-type p58C or mutants was measured by monitoring the change (increase) in fluorescence anisotropy as protein was added to a solution containing 6-carboxyfluorescein labeled DNA (DNA sequence shown in Table S2). The DNA was annealed using a buffer containing 20 mM MES (pH 6.5) and 75 mM NaCl. An increasing concentration (0.1–10 μm) of protein was added to a solution containing 45 nM DNA. Polarized fluorescence intensities were measured using excitation and emission wavelengths of 495 and 520 nm, respectively. Data from three experiments were used to derive the dissociation constants (K_d) by fitting a simple two-state binding model.

The p58C domain contains one solvent exposed tryptophan residue (Trp327), which enables intrinsic tryptophan fluorescence to be used for analyzing interactions involving this residue. Steady-state fluorescence experiments were performed to monitor the effect of binding of the ss/dsDNA junction with eight base pairs and a five-nucleotide 5′ overhang using a SPEX FLUOROMAX spectrofluorimeter operating at room temperature. The excitation wavelength for tryptophan was set to 285 nm and the spectrum was acquired in the range 300–400 nm. The experiments were performed in buffer containing 20 mM MES (pH 6.5) and 50 mM NaCl with a protein concentration of 10–15 μM.

Isothermal titration calorimetry. The wild-type and mutants of p58C were exchanged into 20 mM Tris (pH 7.2) and 75 mM NaCl prior to the experiment. Data were acquired using a MicroCal VP-isothermal titration calorimeter by first injecting 2 μL of 1mM RPA32C into 75 μM p58C contained in the sample cell followed by followed by additional 10 μL injections. The data were analyzed using the Origin software provided by MicroCal. The binding constant (K_d) and thermodynamic parameters were calculated by fitting the data using a nonlinear least-squares fitting algorithm. Single and two-site binding models were tested and the best fits were obtained with the two-site model.

CD spectroscopy. The wild-type and mutants of p58C at 0.3 mg/mL were buffer exchanged into 20 mM MES (pH 6.5) and 50 mM NaCl. The far-UV CD spectrum over the range 200–250 nm was acquired at room temperature using a Jasco J-810 spectrophotometer. Each spectrum is the average of three scans acquired with a scanning rate of 0.2 nm/s.

NMR spectroscopy. Spectra were acquired using Bruker DRX 500, 600, and 800 MHz spectrometers equipped with cryoprobes. ^{15}N-enriched p58C or RPA32C was prepared at 200 μM in a solution containing 20 mM Tris (pH 7.2), 75 mM NaCl, and 2 mM DTT. Two-dimensional ^{15}N-^{1}H heteronuclear single quantum coherence (HSQC) spectra were acquired with 1,024 and 128 complex points in the ^{1}H and ^{15}N dimension, respectively. The titration experiments monitored the chemical shift perturbations of labeled proteins upon successive addition of unlabeled binding partner. Spectra were recorded for labeled:unlabeled protein ratios of 1:0, 1:0.25, 1:0.5, 1:1, and 1:2. Data were processed by Topspin (Bruker) and analyzed with Sparky (University of California).

Computational docking. Unbiased free rigid body docking calculations were performed using Hex (8). The final models were generated using RosettaDock (9), with the two proteins preoriented such that the NMR-identified surface of RPA32C faced the common RPA32C-binding surface of p58C observed in Hex calculations. The final structures were selected based on lowest Rosetta energies.

1. Weiner BE, et al. (2007) An iron-sulfur cluster in the C-terminal domain of the p58 subunit of human DNA primase. *J Biol Chem* 282:33444–33451.
2. Arunkumar AI, et al. (2005) Insights into hRPA32 C-terminal domain—mediated assembly of the simian virus 40 replisome. *Nat Struct Mol Biol* 12:332–339.
3. Otwinowski Z, Minor W (1997) Processing of X-ray diffraction data collected in oscillation mode. *Methods Enzymol* 276:307–326.
4. Vonrhein C, Blanc E, Roversi P, Bricogne G (2007) Automated structure solution with autoSHARP. *Methods Mol Biol* 364:215–230.

5. Emsley P, Cowtan K (2004) Coot: Model-building tools for molecular graphics. *Acta Crystallogr D* 60:2126–2132.
6. Adams PD, et al. (2002) PHENIX: Building new software for automated crystallographic structure determination. *Acta Crystallogr D* 58:1948–1954.
7. Rocchia W, et al. (2002) Rapid grid-based construction of the molecular surface and the use of induced surface charge to calculate reaction field energies: Applications to the molecular systems and geometric objects. *J Comput Chem* 23:128–137.
8. Ritchie DW (2003) Evaluation of protein docking predictions using Hex 3.1 in CAPRI rounds 1 and 2. *Proteins* 52:98–106.
9. Lyskov S, Gray JJ (2008) The RosettaDock server for local protein-protein docking. *Nucleic Acids Res* 36:W233–238.

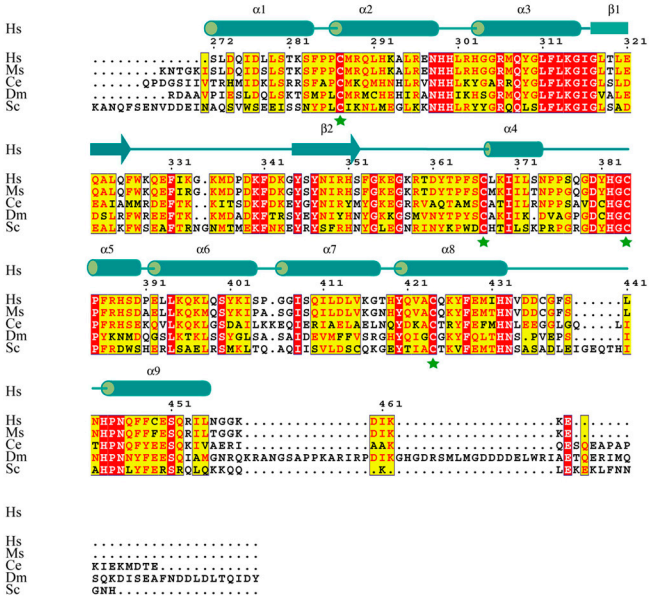

Fig. S1. Multiple sequence alignment of eukaryotic p58C sequences with a schematic of the elements of secondary structure in human p58C colored in green. The conserved residues are colored red and similar residues yellow. The conserved cysteines that chelate the iron-sulfur cluster are marked by green asterisks. Hs, *Homo sapiens*; Ms, *Mouse musculus*; Ce, *Caenorhabditis elegants*; Dm, *Drosophila melanogaster*; Sc, *Saccharomyces cerevisiae*.

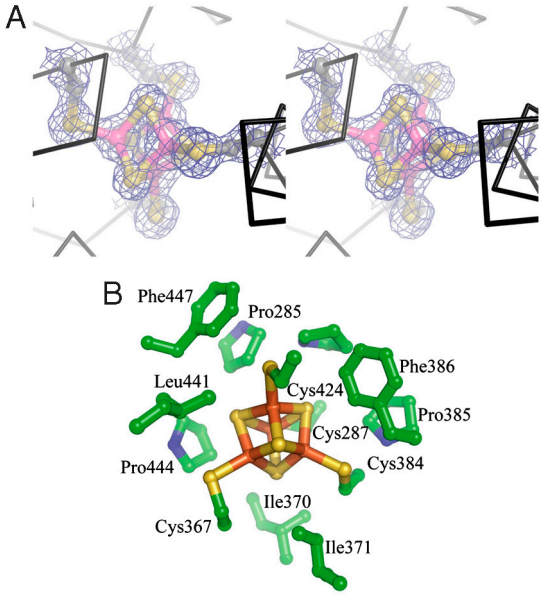

Fig. S2. Structure of the iron-sulfur cluster in p58C. (*A*) The annealed omit 2Fo-Fc electron density map (contoured at 1.0σ) in the vicinity of the iron-sulfur cluster. (*B*) The hydrophobic environment of the iron-sulfur cluster highlighted by showing the side chains of residues surrounding the cluster.

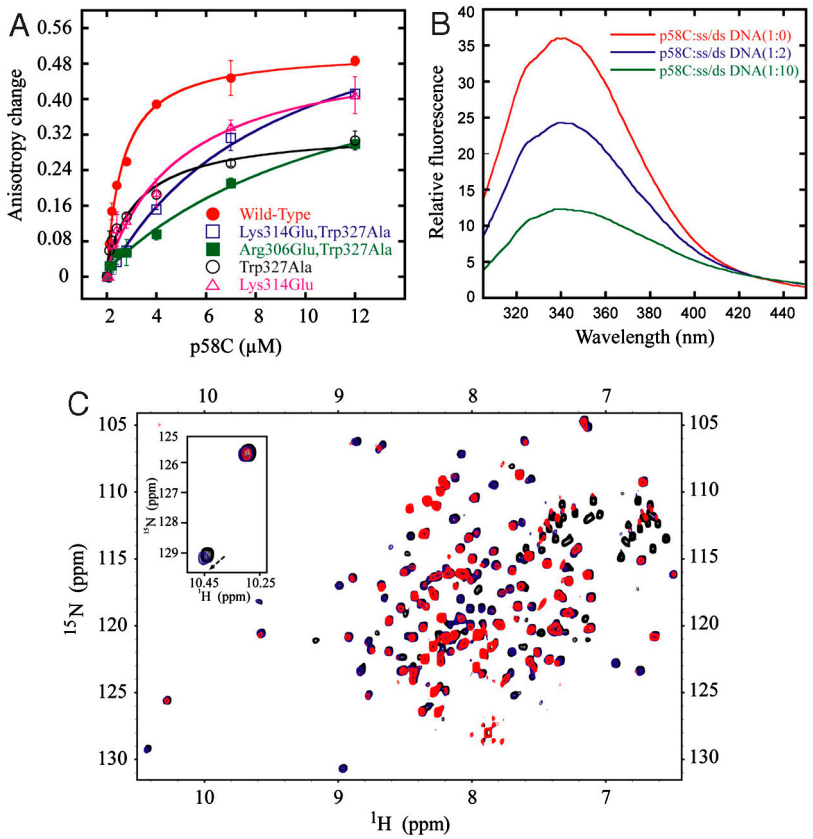

Fig. S3. Comparison the binding of DNA by wild-type and mutant p58C. (*A*) Plot of fluorescence labeled ss/dsDNA junction with eight base pairs and a five-nucleotide 5′ overhang versus concentration of p58C: closed circles, wild-type; open triangles, Lys314Glu; open circles, Trp327Ala; closed squares, Arg306Glu/Trp327Ala; open squares, Lys314Glu/Trp327Ala. Each point is the average of three independent experiments with the standard deviation indicated as the error bar. (*B*) Intrinsic tryptophan fluorescence spectra of p58C in the presence of ss/dsDNA junction at 1 : 0 (red), 1 : 2 (blue), and 1 : 10 (green) molar ratios. (*C*) Overlay of ^{15}N-^{1}H HSQC NMR spectra of p58C in the absence (black) and presence of 1 : 0.25 (blue), and 1 : 0.5 (red) molar ratios of the ss/dsDNA junction. The inset shows an expansion of the downfield region of the spectrum containing the NH signal from the tryptophan ring and one low-field backbone amide. The arrow indicates the chemical shift perturbation of the Trp residue.

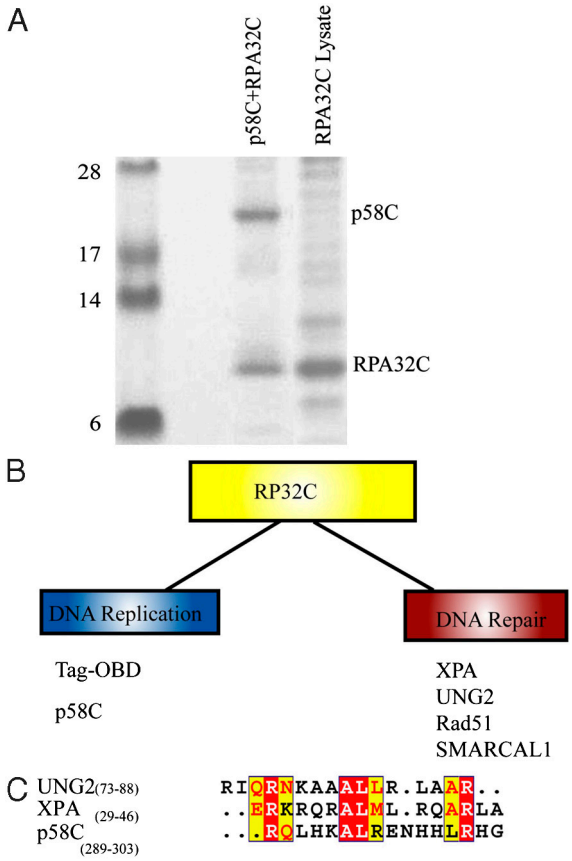

Fig. S4. Interactions with RPA32C. (*A*) Binding of p58C to RPA32C detected by pull-down using cell lysate containing recombinant RPA32C incubated with His-tagged p58C bound to nickel beads. The bound protein was eluted and identified by SDS-PAGE. (*B*) Schematic diagram showing known interactions of RPA32C with other proteins involved in DNA replication and repair. (*C*) Multiple sequence alignment of RP32C binding regions of XPA and UNG2 with p58C. Invariant residues are shaded in yellow and conserved residues in red.

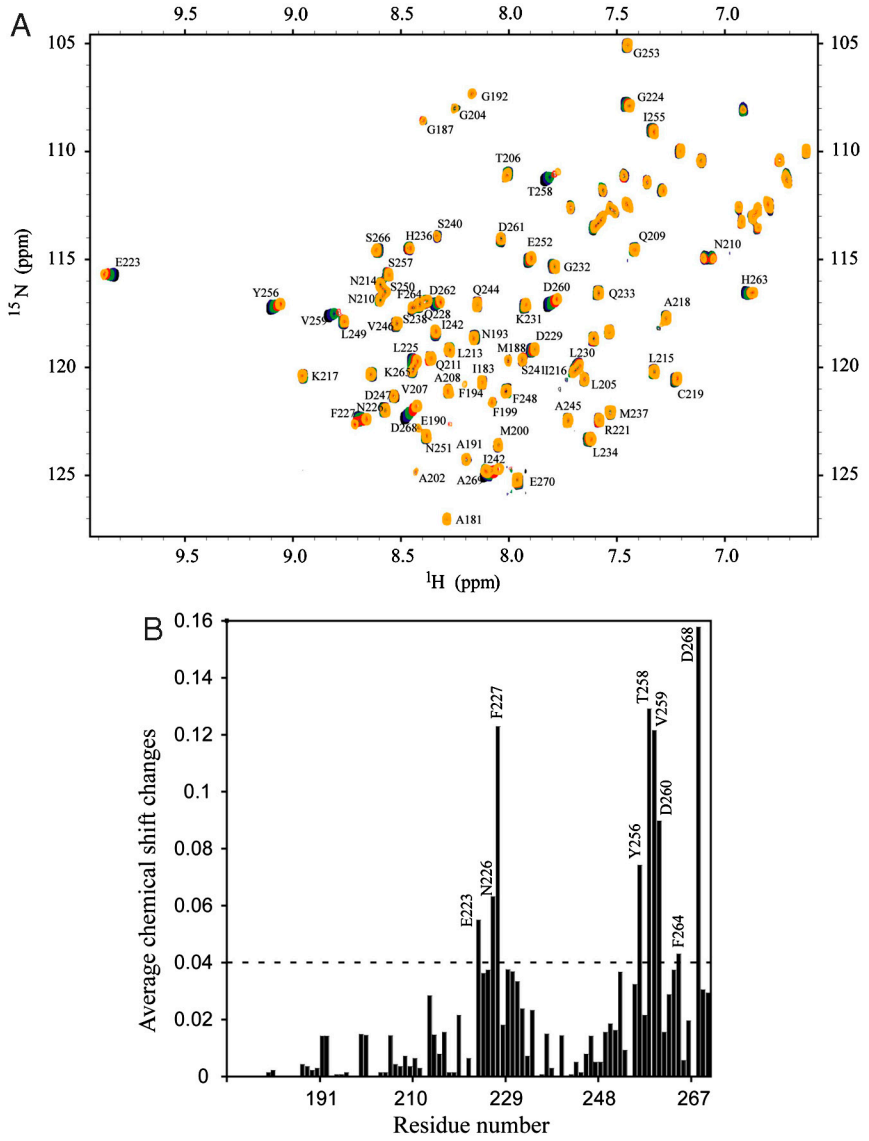

Fig. S5. NMR analysis of the interaction of p58C with RPA32C. (*A*) ^{15}N-^{1}H HSQC spectra acquired for ^{15}N-RPA32C in the absence (black) and presence of 1:0.25 (purple), 1:0.5 (green), 1:1 (red), and 1:2 (yellow) molar ratios of p58C. (*B*) Plot of NMR chemical shift perturbation versus residue number upon titration of p58C into RPA32C. The data were analyzed using the equation, $\Delta\delta = [(\Delta\delta_{HN})^2 + (\Delta\delta_N/6.5)^2]^{1/2}$. The dashed line represents the mean chemical shift perturbation.

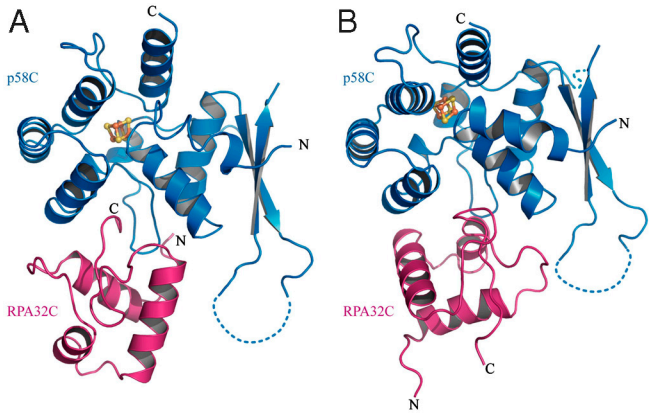

Fig. S6. Ribbon representation of the two families of p58C–RPA32C complexes predicted by Hex (8).

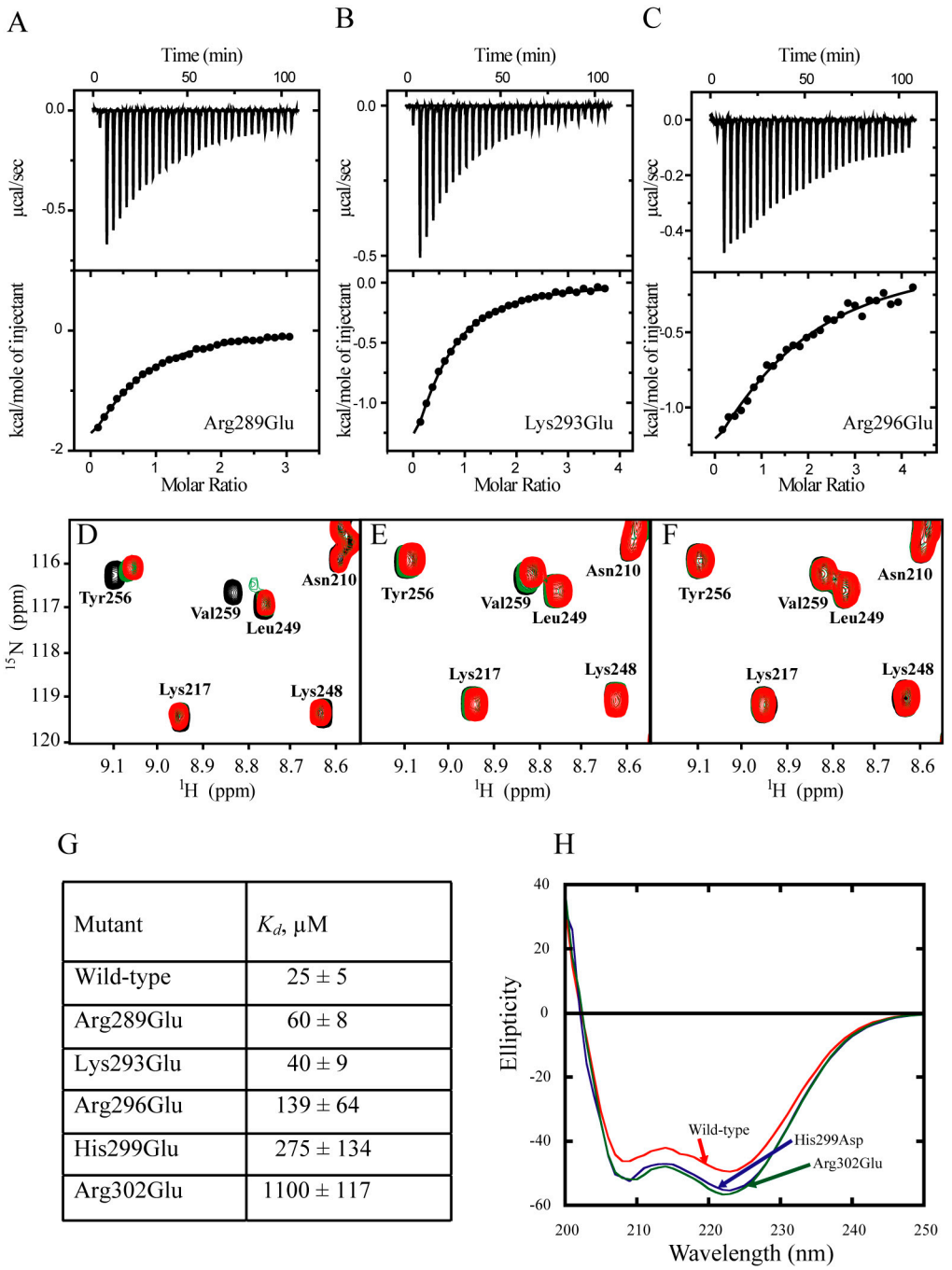

Mutant	K_d, µM
Wild-type	25 ± 5
Arg289Glu	60 ± 8
Lys293Glu	40 ± 9
Arg296Glu	139 ± 64
His299Glu	275 ± 134
Arg302Glu	1100 ± 117

Fig. S7. Characterization of the RPA32C binding properties and structure of p58C mutants. (*A–C*) Isothermal titration calorimetry of the interaction of RPA32C with p58C mutants Arg289Glu (*A*), Lys293Glu (*B*), and Arg296Glu (*C*). The upper panel shows raw heat release upon addition of RPA32C onto solutions containing p58C mutants. The lower panel shows the integrated raw injection points. (*D–F*) ^{15}N-^{1}H HSQC NMR spectra of ^{15}N-enriched RPA32C acquired at molar ratios of 1:0 (black), 1:1 (green), and 1:2 (red) using wild-type (*D*), His299Asp (*E*), and Arg302Glu (*F*) p58C. (*G*) Table containing dissociation constants determined by isothermal titration calorimetry for the binding of RPA32C to p58C wild-type and mutants. (*H*) Far UV CD spectra of p58C wild-type (red), Arg302Glu (green), and His299Asp (blue).

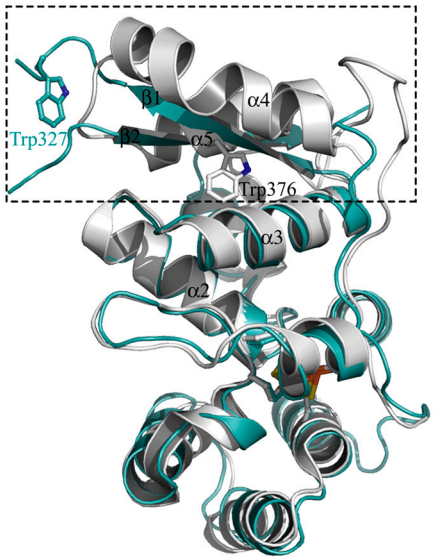

Fig. S8. Comparison of the structure human p58C with yeast PriL-CTD. The structure of human p58C (PDB ID code 3L9Q, cyan) is superimposed on the yeast PriL-CTD structure (PDB ID code 3LGB, gray). The structurally dissimilar region is highlighted with the dotted box. The conserved tryptophan is shown in ball and stick representation.

Table S1. Crystallographic data collection and refinement statistics for p58C

	Native	Fe SAD
Cell parameters		
a	109.44 Å	109.31 Å
b	53.05 Å	52.73 Å
c	88.84 Å	88.73 Å
α	90.00	90.00
β	115.09	115.16
γ	90.00	90.00
Space group	C2	C2
Molecules/asu	2	2
Data collection		
Wavelength, Å	0.97872	1.54188
Resolution, Å	46.8–1.7	46.5–2.1
Completeness, %	97.5 (84.9)	92.5 (55.3)
Redundancy	7.1 (5.7)	7.9 (0.7)
R_{sym}	0.074 (0.238)	0.074 (0.171)
$\langle I \rangle / \langle \sigma_I \rangle$	21.2 (6.9)	16.6 (2.0)
Refinement		
Resolution, Å	1.7	
No. reflections	49,670	
R_{cryst}/R_{free}	0.130/0.169	
No. atoms		
Protein/solvent	2,846/464	
Avg B factor, Å^2		
Protein/solvent	27.12/45.2	
rmsd bonds, Å	0.005	
rmsd angles, °	0.920	
Ramachandran Statistics, %		
Most favored	93.7	
Additionally allowed	6.3	
PDB ID code	3L9Q	

Values in parentheses refer to the highest resolution shell; asu, asymmetric unit.

Table S2. DNA binding affinities of wild-type and mutant p58C

Oligonucleotide, (WT-p58C)	K_d, μM	*DNA substrate*
5′ ss/dsDNA–RNA (8 base pair duplex)	0.34 ± 0.09	*TCTCTCTCTCAAA-3′ GAGAGUUU-5′
5′ ss/dsDNA (8 base pair duplex)	0.30 ± 0.12	*TCTCTCTCTCAAA-3′ GAGAGTTT-5′
5′ ss/dsDNA (12 base pair duplex)	0.21 ± 0.07	*TCTCTCTCTCAAATCTCC - 3′ AGAGTTTAGAGG - 5′
5′ ss/dsDNA (20 base pair duplex)	0.20 ± 0.05	*CTCTCTCTCTCTCTCAAATCTCC - 3′ AGAGAGAGAGAGTTTAGAGG - 5′
3′ ss/dsDNA (8 base pair duplex)	0.40 ± 0.18	*CCTCTCAACTCTCT - 3′ 5′-GGAGAGTT
dsDNA 12-mer	1.3 ± 0.3	*CTCTCTCTCAAA - 3′ GAGAGAGAGTTT - 5′
ssDNA 7-mer	95 ± 15	*TCTCTCT - 3′
ssDNA 12-mer	2.9 ± 1.52	*CCTCAACTCTCT- 3′
Mutant p58C	***K_d, μM***	***DNA substrate***
His299Asp	0.3 ± 0.2	*TCTCTCTCTCAAA-3′ GAGAGTTT-5′
Arg302Glu	3.4 ± 1.5	
Lys314Ala	1.2 ± 0.1	
Lys314Glu	3.2 ± 1.1	
Trp327Ala	1.4 ± 0.2	
Lys328Ala	0.4 ± 0.1	
Lys369Ala	0.5 ± 0.1	
Arg306Glu,Trp327Ala	10.2 ± 3.4	
Lys314Glu,Trp327Ala	6.8 ± 1.2	